ChemPubSoc Europe
DOI: 10.1002/cphc.201500237
CHEMPHYSCHEM
Articles

Phase Coexistence in a Dynamic Phase Diagram

Luigi Gentile,*[a, b] Luigi Coppola,[a] Sandor Balog,[c, d] Kell Mortensen,[e] Giuseppe A. Ranieri,[a] and Ulf Olsson[b]

Metastability and phase coexistence are important concepts in colloidal science. Typically, the phase diagram of colloidal systems is considered at the equilibrium without the presence of an external field. However, several studies have reported phase transition under mechanical deformation. The reason behind phase coexistence under shear flow is not fully understood. Here, multilamellar vesicle (MLV)-to-sponge (L_3) and MLV-to-L_α transitions upon increasing temperature are detected using flow small-angle neutron scattering techniques. Coexistence of L_α and MLV phases at 40 °C under shear flow is detected by using flow NMR spectroscopy. The unusual rheological behavior observed by studying the lamellar phase of a non-ionic surfactant is explained using ^{2}H NMR and diffusion flow NMR spectroscopy with the coexistence of planar lamellar–multilamellar vesicles. Moreover, a dynamic phase diagram over a wide range of temperatures is proposed.

1. Introduction

An equilibrium phase diagram demarcates areas of existence of various phases typically as a function of temperature and concentration. The term “equilibrium” refers to the microstructural level. The equilibrium phase diagrams of lyotropic liquid crystals are complex because of the many possible phase regions, according to Gibbs’ phase law.[1] In some cases, even three phases can coexist.[2] Examples of lyotropic-phase structures are the fluid lamellar L_α phase, in which sheets of bilayers are separated by bulk liquid, or the sponge L_3 phase, in which an organized bilayer is arranged in a random, isotropic configuration.[3,4]

There is a strong correlation between microstructure and mechanical properties, however the presence of a mechanical field is usually not considered in the phase diagrams. The term “dynamic” is used to refer to an equilibrium phase diagram that also considers the effect of the shear flow.[5] Whereas dynamic phase diagrams are still not common in the literature, considerable work has been done on ethylene oxide non-ionic surfactants. In particular, the dynamic phase diagrams of triethylene glycol decyl ether ($C_{10}E_3$), and triethylene glycol dodecyl ether ($C_{12}E_3$) and tetraethylene glycol hexadecyl ether ($C_{16}E_4$) in D_2O have been reported.[5–7] The L_α phase of these systems shows a strong nonlinear response to the applied deformation, that is, shear flow. Experimentally, three main orientations of the lamellae under flow have been found:[8] 1) the “parallel” orientation (also called the *c* orientation), in which the normal of the lamellar planes is parallel to the velocity gradient direction; 2) the “perpendicular” orientation (*a* orientation), in which the normal of the lamellae is parallel to the vorticity (neutral) direction; and 3) the “transpose” orientation (*b* orientation), in which the normal is parallel to the shear flow direction. Mixtures of *c* and *a* orientations have been observed under shear flow.[9–11] Moreover, closed structures identified as multilamellar vesicles (MLVs) can be formed under shear flow.[5–32] The mechanism of MLV formation was described in detail[30] by using the 1–2 shear cell[33,34] in time-resolved small-angle neutron scattering experiments (SANS). The 1–2 shear cell allows the 2D pattern in the velocity–velocity gradient plane to be recorded, that is, for the first time the transition was observed looking at the *c* orientation of the lamellar phase such that it should be the principal orientation after the alignment procedure.

Other shear-induced transitions are possible, for instance the L_3 phase under shear in a Couette cell can be completely transformed into a lamellar phase L_α above a critical shear rate[35,36] that can subsequently lead to a lamellar-to-MLV transition.[37] Moreover, a gyroid-to-cylinder transition is reported for diblock copolymers,[38] in which cylinders can be hexagonally packed.[39]

As the existence and properties of equilibrium-phase coexistence is of interest, the focus of this paper is phase coexistence regions in the dynamic phase diagram and also the relative stability of the formed microstructure after the applied deformation. Here, the metastability of a non-ionic lamellar phase ($C_{12}E_3$ in D_2O) is considered after shear flow deformation. It is

---

[a] *Dr. L. Gentile, Prof. L. Coppola, Prof. G. A. Ranieri*
Department of Chemistry and Chemical Technology
University of Calabria
P. Bucci 14C, 87036 Rende (Italy)
E-mail: luigi.gentile@unical.it

[b] *Dr. L. Gentile, Prof. U. Olsson*
Physical Chemistry Division
Chemistry Department, Lund University
P.O. Box 124, 221 00 Lund (Sweden)

[c] *Dr. S. Balog*
Laboratory for Neutron Scattering
Paul Scherrer Institut
5232, Villigen (Switzerland)

[d] *Dr. S. Balog*
Adolphe Merkle Institute
University of Fribourg
1700 Fribourg (Switzerland)

[e] *Prof. K. Mortensen*
Niels Bohr Institute
University of Copenhagen
2100 Copenhagen (Denmark)

essential to determine the phase coexistence in order to know the thermodynamic state of the system. ^{2}H NMR and diffusion flow NMR spectroscopy were used to identify the coexistence phases. Moreover, a correlation between molecular structure and the formation of multilamellar vesicles can be established through the metastability of their lamellar phases under shear flow. The phase coexistence under shear flow has been reported for $C_{12}E_3$ in D_2O,[6,7] however there is no explanation for such evidence. Olmsted and Lu[40] reported an interesting hypothesis on the phase coexistence under flow. Here, several pieces of information are given in order to understand better the mechanism behind the coexistence under flow. This study also extends the dynamic phase diagrams of the $C_{12}E_3$ surfactant at a higher temperature than previously reported,[6] where the static phase diagram shows a lamellar and sponge phase coexistence.

2. Results and Discussion

The phase-transition temperatures of 40 wt% $C_{12}E_3$ in D_2O can be obtained from the $C_{12}E_3$–H_2O phase diagram proposed by Laughlin,[41] by calculating the corresponding surfactant concentration in D_2O. The L_α exist at temperatures up to $40.0\pm0.5\,^\circ$C, and an L_3–L_α coexistence is reported in the temperature range 40–$48.2\pm0.5\,^\circ$C.[41] L_3 exists from 48.2 to $52.0\pm0.5\,^\circ$C, with L_3–L_α coexistence until $57.9\pm0.5\,^\circ$C. The steady-state viscosities are shown in Figure 1 as functions of shear rate ranging from 0.1 to 100 s^{-1}, for a system with 40 wt% $C_{12}E_3$ in D_2O at 24, 34 and 40 °C. Three regimes can be observed in all flow curves: the first regime is almost a plateau at 24 and 34 °C, whereas shear thinning is observed at 40 °C. This shear-thinning regime is expected to originate from orientation or alignment of the lamellar phase in the flow direction as previously observed at the same temperature for the 50 wt% $C_{12}E_3$–D_2O system.[6,22] The second regime is a shear thickening at all temperatures, however this regime appears at a relatively high value of shear at 40 °C; this transition regime is usually ascribed to the formation of MLV.[6,16] The results are in agreement with the dynamic phase diagram of the surfactant,[6] except for the transition region, which was slightly modified. The third regime shows shear-thinning behavior, in agreement also with the previous studies on $C_{10}E_3$–D_2O,[5] and this can be described well by a power-law relation. In particular, $\eta = \dot{\gamma}^{(-0.71\pm0.03)}$, $\eta = \dot{\gamma}^{(-0.45\pm0.04)}$ and $\eta = \dot{\gamma}^{(-0.5\pm0.1)}$ at 24, 34 and 40 °C, respectively. The shear-thinning exponent at 24 °C is comparable with the exponent obtained at the same temperature but at 50 wt% (-0.6 ± 0.1). Moreover, an exponent of -0.8 was observed in an dioctyl sodium sulfosuccinate-based system[14] and for $C_{16}E_4$–D_2O.[7] On the contrary, at 40 °C, the exponent is not consistent with that recorded at 50 wt% surfactant (-0.67 ± 0.01), although for a $C_{10}E_3$–D_2O system,[5] an exponent equal to -0.5 was observed. The shear-thinning regime is associated with densely packed MLVs.[42] Similarities in the slope might be related to differences in the densely packed structures. However, the result at 40 °C suggests a dissimilarity with this description. In order to understand this behavior the water self-diffusion in the three axes and ^{2}H NMR experiments were performed. The axes were: D^z along the vorticity direction, D^y along the velocity direction and D^x along the velocity gradient direction. The *z*, *y* and *x* directions are shown in Figure 2 (inset). For more details, see the Experimental Section.

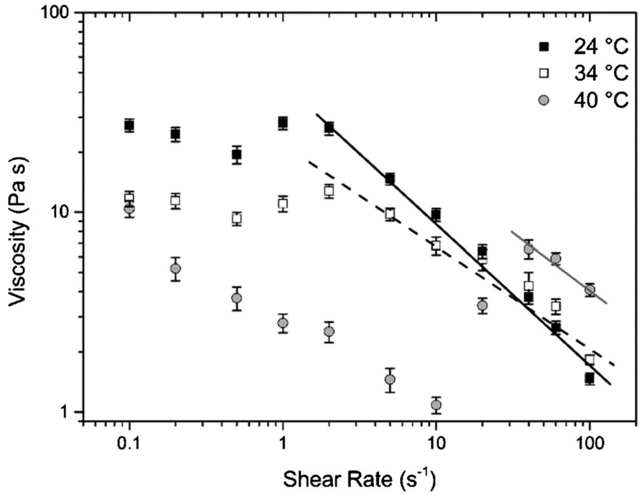

Figure 1. Steady-state viscosity as a function of the shear rate at 24, 34 and 40 °C. Rheological data were obtained after transient experiments at fixed shear rates in the steady state for 40 wt% $C_{12}E_3$ in D_2O. The solid and dashed lines show a power law relation. Before the transient experiments, a shear rate of 10 s^{-1} was applied for 1 h to the lamellar phase at 55 °C in order to have a *c* orientation as the initial state.

Medronho et al.[13,28] reported the evolution of the water self-diffusion coefficient *D*, with strain for the three spatial directions during MLV formation. Initially, the lamellar phase shows a D^x value of more than one order of magnitude smaller than D^z and D^y. This is due to the alignment of layers of the la-

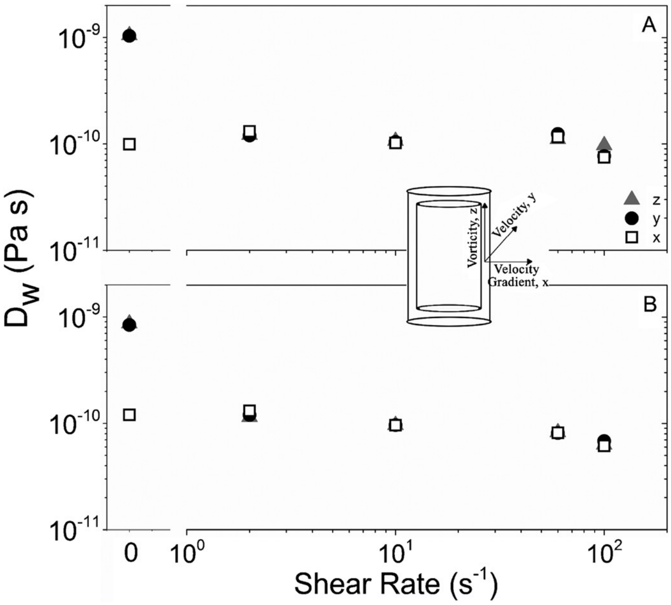

Figure 2. Diffusion coefficients along the velocity, vorticity, and velocity gradient directions after the transient experiments performed in situ at 2, 10, 60 and 100 s^{-1} at 24 °C (A) and 34 °C (B). The diffusion coefficients reported at shear rate 0 s^{-1} were obtained after alignment of the lamellar phase. Each transient experiment was performed after the alignment procedure.

mellar phase along the flow direction. The initial state of the $C_{12}E_3$ lamellar phase was obtained by applying a shear rate of $10\,s^{-1}$ for 1 h at 55 °C in the experiments performed here. Figure 2 shows the water self-diffusion coefficients obtained after the applied shear deformation, that is, after the transient experiments at 2, 10, 60 and $100\,s^{-1}$ at 24 and 34 °C. However, the D values reported at the shear rate of $0\,s^{-1}$ were measured after the alignment procedure described previously; indeed it represents the initial state. A D^x value one order of magnitude smaller than D^z and D^y is characteristic of the initial state. Although the diffusion coefficients along the three directions are almost identical after the transient experiments performed in situ, a slight decrease of the coefficients with shear rate was observed.

Figure 3 reports the water self-diffusion coefficients obtained after the transient experiments at 2, 10, 60 and $100\,s^{-1}$ at 40 °C. One can easily observe the differences between the diffusion coefficients reported in Figures 2 and 3. D^x is more than one order of magnitude smaller than D^z and D^y after the transient experiments at $2\,s^{-1}$, whereas after $10\,s^{-1}$, D^x is almost two orders of magnitude smaller than D^z and D^y. These results suggest a full alignment of the lamellar layers in the direction of the flow, as is suggested by the flow curve at 40 °C (Figure 1). Moreover, after the transient experiment at $60\,s^{-1}$ it was not possible to obtain convergence fitting of the data with Equation (1) ($k=2$), although it was possible by using a value of $k=3$:

$$I = I_0 \sum_{n=1}^{k} f_n e^{\left[-D_n(\gamma\delta g)^2\left(\Delta-\frac{\delta}{3}\right)\right]} \tag{1}$$

where I and I_0 represent the water resonance peak intensity in the presence and absence of field gradients, γ is the proton gyromagnetic ratio, f_n is the weighting of the n value, Δ is the time between the start of the gradient pulses of amplitude g, and duration δ. The diffusion coefficients along the three axes with lower values of f_n were not considered because they are related to sample inhomogeneity, whereas the other coefficients were considered in two triplets of values together with the f_n value (see also the Experimental Section). From the results obtained it is evident that the phase coexistence that can be assumed between planar lamellae is partially aligned to the flow—as D^x is smaller than D^y and D^z—and MLVs. Finally, after the transient experiment at $100\,s^{-1}$ the MLVs were formed.

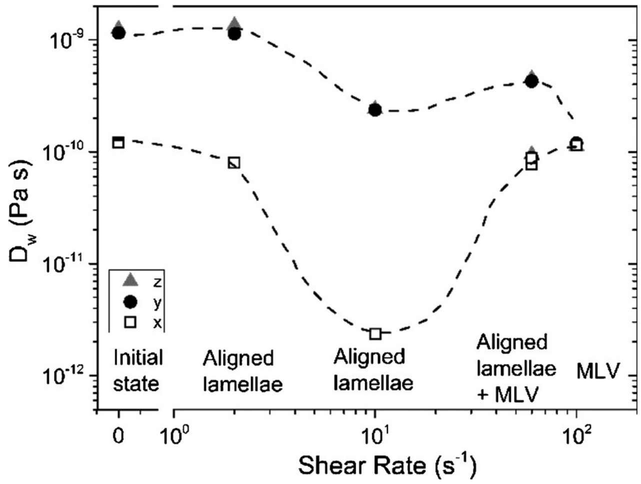

Figure 3. Diffusion coefficients at 40 °C along the velocity, vorticity, and velocity gradient directions after the transient experiments performed in situ at the same shear rates shown in Figure 2. The diffusion coefficients reported at shear rate $0\,s^{-1}$ were obtained after alignment of the lamellar phase. Each transient experiment was performed after the alignment procedure. There are two triplet values of diffusion coefficient for $60\,s^{-1}$, as in this case there was no convergence in the fitting with $k=2$, and therefore $k=3$ was used.

Figure 4 shows the ^{2}H NMR spectra recorded before (at $0\,s^{-1}$) and after the transient experiments (at 2, 10, 60 and $100\,s^{-1}$). As discussed above, the initial state was obtained by applying a shear rate of $10\,s^{-1}$ for 1 h at 55 °C. The Pake doublet of a lamellar phase is observed as an initial state, however the lamellae are not completely aligned to the flow, as it is apparent that the distance between D^x and $D^{z,y}$ is smaller compared to the aligned state of the $C_{10}E_3$ lamellar phase.[13] The width at half-height of the singlet due to the MLVs decrease as a function of the shear rate and temperature, as one might expect as the MLV size also decreases as a function of these parameters.[7,23,24] At 40 °C, the assumption from the diffusion experiments is confirmed, as the ^{2}H NMR spectra at 2 and $10\,s^{-1}$ can be related to a well-aligned lamellar phase. This happens also in the case of the $C_{10}E_3$ system[13,28] between 38 and 40 °C. However, in the case of $C_{10}E_3$, the lamellar phase persists also at high shear rates; at the end of the transient experiment at $60\,s^{-1}$ the lamellar–MLV phase coexistence was confirmed. Moreover, at $100\,s^{-1}$ MLVs were formed. It is notable that at 24 °C and after 2 and $10\,s^{-1}$, the width at half-height of the quadrupolar spectrum is of the order of the peak–peak distance of the lamellar phase. This could be due to 1) larger vesicles than in the other experiments, 2) coexistence between the planar lamellae and vesicles, or 3) an incomplete transition that leads to multilamellar cylinders.[13] However, the experiment after $2\,s^{-1}$ is still in the transition region of the dynamic phase diagram.[6] At the end of the transient experiments the spectra were monitored for one day, and no change was observed except in the spectra recorded after $60\,s^{-1}$. Figure 5 shows the ^{2}H NMR spectra recorded after the deformation. The lamellar fractions increase over time, reaching a stability (in the observed time) after 8 h. Phase coexistence is stable also several hours after the applied deformation. The shear-induced phase coexistence is an important concept to be focused on, not only from a fundamental point of view but also for possible applications.

The scattering profiles under shear rates of 10 and $60\,s^{-1}$ were recorded for 40 wt % surfactant at 47 °C (Figure 6). The experiments were performed after the formation of MLVs at lower temperature. At 47 °C, the static phase diagram reveals a lamellar–sponge phase coexistence. The shear rate of $10\,s^{-1}$ affects the equilibrium state of coexistence giving MLVs, whereas at $60\,s^{-1}$ the planar lamellae dominate. These results allow extension of the dynamic phase diagram previously published; in fact the lamellar-sponge coexistence disappears.

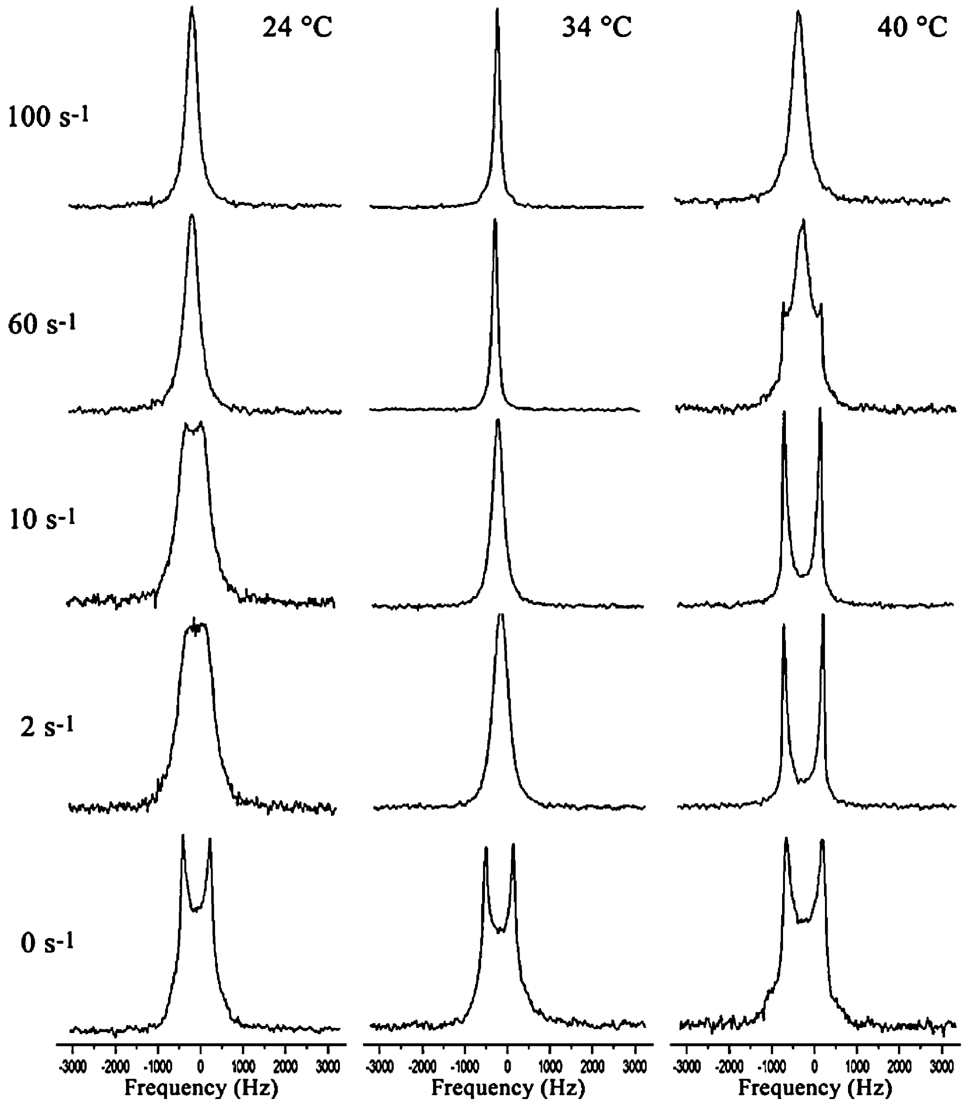

Figure 4. ^{2}H NMR spectra recorded before (at 0 s^{-1}) and after the transient experiments (at 2, 10, 60 and 100 s^{-1}). The initial state was obtained by applying a shear rate of 10 s^{-1} for 1 h at 55 °C. The spectra recorded at the beginning of each transient experiment were the same. The experiments shown were recorded before the 2 s^{-1} experiments.

Upon increasing the temperature from 47 to 55 °C at 10 s^{-1}, the amount of sponge phase increases and the MLV fraction decreases. The time transition between MLVs and the L_3 steady state goes first through a two-phase coexistence in which an L_3 phase coexists with the L_α. In fact, Figure 7 A reveals the isotropic scattering of the sponge phase and shows two peaks in the neutral direction due to a lamellar phase. As a comparison, in Figure 7 B the steady state is shown. The data provide a picture of the transition from MLVs to L_3. MLVs become a lamellar phase, which is not stable under shear and results in the L_α-to-L_3 transition. At 60 s^{-1}, the L_3 phase is disfavored due to the higher deformation applied, as the reverse transition from L_3 to L_α appears.

Phase coexistence was reported between the end of the shear thickening and the beginning of the shear-thinning behaviour, that is, at relatively high shear rates. The rheology experiments were performed in step-rate experiments such that the shear rate was constant. Theoretically, it could be possible to maintain a stable stress on the two-state region during these experiments. In practice, this would also seem to be difficult. Olmsted and Lu[40] determined phase coexistence by constructing a stable coexisting steady state, which requires inhomogeneous terms in the equations of motion for a given shear rate. They discussed the phase diagrams for common stress coexistence, in which the phase separation is radial in a cylindrical Couette flow. For common stress phase coexistence of two phases, in this case L_α and MLV, is determined by the lever rule [Eq. (2)]:

$$\dot{\gamma} = \phi_{L\alpha}\dot{\gamma}_{L\alpha} + (1 - \phi_{L\alpha})\dot{\gamma}_{\mathrm{MLV}} \qquad (2)$$

where $\phi_{L\alpha}$ is the planar lamellae fraction.

Olmsted and Lu suggested that the composition can be the reason for an unstable flow under controlled shear rate conditions. The results reported here suggest that phase coexistence is also strongly related to the temperature. The lyotropic liquid crystal structures show several values of bending and saddle-splay moduli that change with concentration or temperature.[7] As a consequence, a common stress phase separation can be stable under certain conditions. Moreover, in a Couette device the slight inhomogeneity of the flow induces asymmetry between the inner and outer cylinders, exactly the symmetry of common stress phase separation. The lyotropic structures having certain resistance to the applied flow can reach steady states by which two phases coexists due to slight inhomogeneity of the flow in the gap.

The $C_{12}E_3$ dynamic phase diagram[6] was implemented by adding the phase MLVs and L_α coexistence individuated at 60 s^{-1} and 40 °C, and it was also extended at higher temperature. Figure 8 reports the dynamic phase diagram at 40 wt % surfactant, together with static equilibrium phases reported by Laughlin[41]

3. Conclusions

The $C_{12}E_3$ dynamic phase diagram[6] shows a stable lamellar phase under shear flow below 60 s^{-1} at 40 °C; by increasing

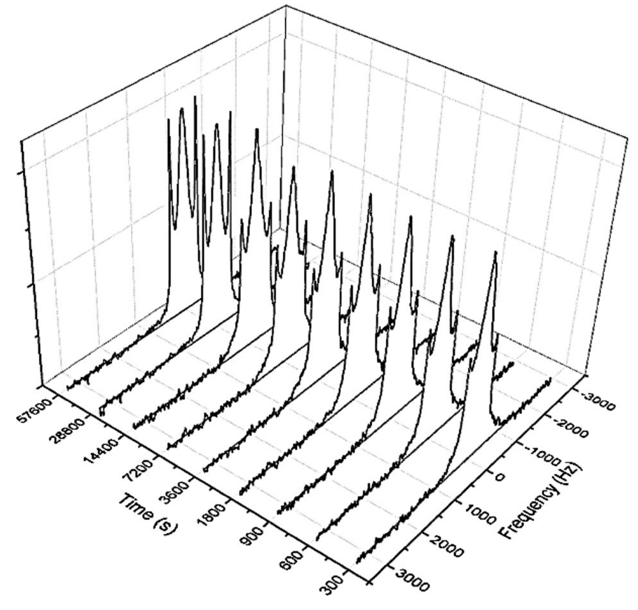

Figure 5. ^2H NMR spectra recorded after the transient experiment at 60 s^{-1}.

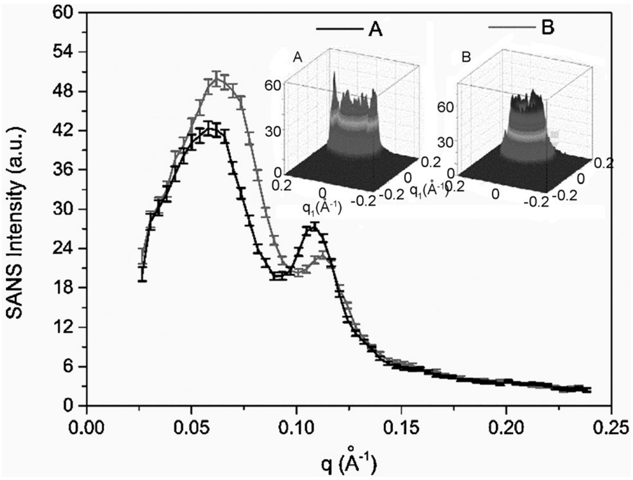

Figure 7. SANS profiles detected in the radial beam configuration at 55 °C under a constant shear rate of 10 s^{-1}, that is, the patterns were recorded during the transition. A) L_3–L_α transitional state, B) L_3 steady state. Inset: corresponding 3D patterns.

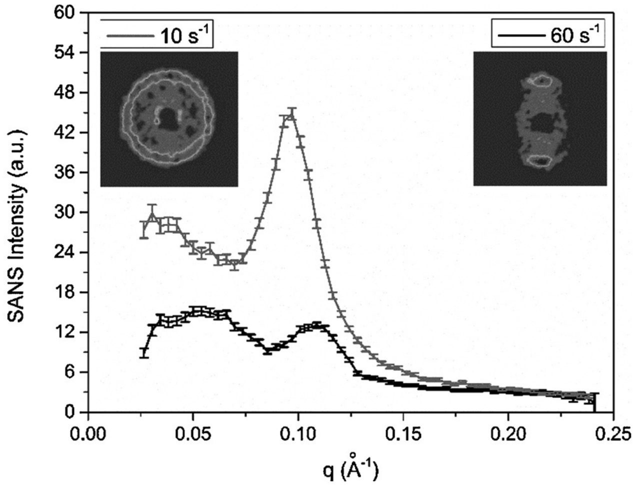

Figure 6. SANS profiles under a shear rate of 10 and 60 s^{-1} at 40 wt% surfactant, 47 °C. Inset: corresponding 2D patterns.

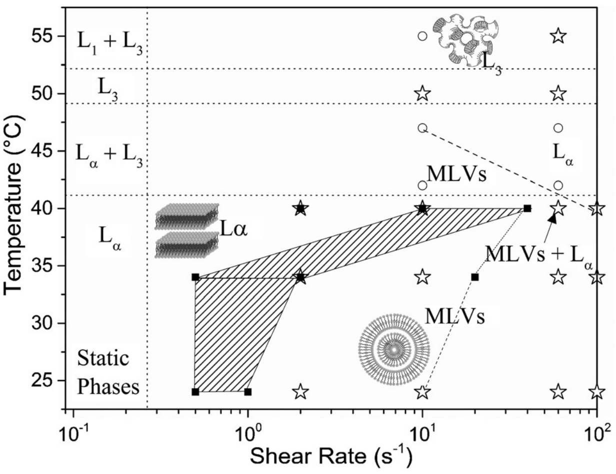

Figure 8. Dynamic phase diagram of 40 wt% $C_{12}E_3$ in D_2O. Open circles indicate SANS data, black squares indicate rheological data, and open stars indicate ^2H and water self-diffusion data. On the left the equilibrium static phases are reported.[42]

the shear rate, MLV formation occurs. Water self-diffusion and ^2H NMR experiments at 60 s^{-1} and 40 °C show multilamellar vesicles and L_α coexist in a *c* orientation. Moreover, the viscosities of the $C_{12}E_3$–D_2O system at 40 wt% surfactant were reported in the flow curves at 24, 34 and 40 °C. The static phase diagram shows a lamellar–sponge phase coexistence at 47 °C and an L_1–L_α coexistence at 55 °C, whereas time-resolved flow SANS experiments at 10 s^{-1} show that MLVs still dominate at 47 °C, whereas L_3 dominates at 55 °C. Moreover, a phase coexistence between L_3 and L_α was detected during the MLV-to-L_3 transition upon increasing the temperature from 47 to 55 °C. Finally, an extended dynamic phase diagram for the $C_{12}E_3$–D_2O system at 40 wt% surfactant was proposed.

The dynamic phase diagram of the $C_{10}E_3$–D_2O is reported[5] and shows a stable lamellar phase in the *c* orientation for temperatures of less than 40 °C. At lower temperatures, the lamellar structure is unstable under shear flow, and MLV formation already occurs at a few reciprocal seconds. No phase coexistence was reported. The dynamic phase diagram of the $C_{16}E_4$–D_2O system exhibits L_α and L_3, and at higher shear rates, MLV and L_3 phases coexist at high temperature.[7]

Here, several insights on the complex matter of phase coexistence under shear flow were reported. This is an interesting topic for further investigations, as it represents a point of balance between the equilibrium and the dynamic microstructure. Establishing an equilibrium for two systems being in contact requires mechanical, thermal and chemical equilibria to be achieved.

Experimental Section

Materials

The triethylene glycol dodecyl ether ($C_{12}E_3$) was purchased from Nikko Chemicals Co., Ltd. (Tokyo, Japan). Deuterium oxide (D_2O) was purchased from Armar Chemicals (Döttingen, Switzerland). The purity of each material was higher than 99.8%, and the materials were used without further purification. Samples containing 40 wt% surfactant were prepared by mixing the surfactant and D_2O. The mixing was assisted by gentle stirring, and the mixtures were left overnight. The $C_{12}E_3$–water phase diagram proposed by Laughlin[41] is qualitatively different from that previously reported in the literature,[43] in which the existence of a sponge phase was not identified. The system showed a wide lamellar phase at low temperature, between 24 and 40 °C. At high temperature, the system showed a lamellar–sponge phase coexistence.

^{2}H Flow NMR

Experiments were performed on ^{2}H nuclei before and after the applied in situ shear flow, using a cylindrical cuvette having 9.0 mm inner radius and 1.0 mm gap. The cell was integrated in a microimaging probe of a wide-bore superconducting magnet. The long axis of the cuvette was parallel to the magnetic field director. Shear was applied by rotating an inner cylinder fitted in the cuvette (Figure 9). An external step-motor gearbox, mounted on the top of the magnet, drove the cylinder motion. ^{2}H spectra were measured on a Bruker Avance 300 spectrometer, working at 46.073 MHz recorded. ^{2}H NMR is a sensitive technique to for analyzing lyotropic liquid crystals, providing relevant information on the microstructure[44–46] also under shear flow.[13,15,28,29]

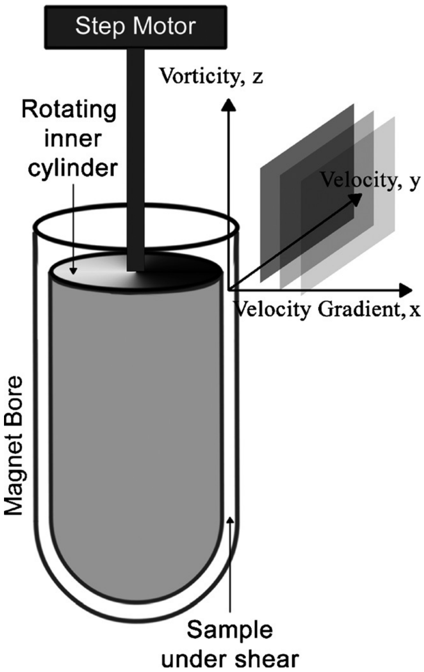

Figure 9. Flow NMR Couette scheme and the related shear frame of coordinates with velocity, vorticity, and velocity gradient directions. Depicted in the axis frame is an aligned lamellar phase in the direction of the flow (*c* orientation).

Diffusion Flow NMR

Self-diffusion coefficients were measured using a microimaging probe having a three-axis gradient facility and a maximum gradient strength of 100 G cm^{-1} on a Bruker Avance 300 spectrometer operating at 300.0 MHz (^{1}H nuclei). The diffusion experiments were performed using the longitudinal eddy-current delay–pulse gradient stimulated echo (LED–PGSTE) sequence.[47] LED is a method for avoiding eddy-current artefacts that involves placement of an eddy-current delay after the application of a gradient pulse. In this case, a delay of 6 ms was used for all experiments. In the LED–PGSTE sequence, as well as in the PGSTE, a pair of trapezoidal narrow magnetic field gradient pulses with amplitude g and duration δ encode for spin displacement over a controlled observation time Δ. By applying the pulsed magnetic field gradients in the x, y or z direction, the corresponding diffusion coefficient can be determined. The optimal experimental conditions were $\Delta = 20$ ms, $\delta =$ 2 ms and $\Delta = 40$, $\delta = 4$ ms for the lamellar phase and MLV state, respectively, whereas g values were varied from 4.9 to 97.8 G cm^{-1}, in 16 gradient steps. The spin-echo decays were analyzed according to the method of Stejskal and Tanner,[48] however some of the acquired data did not fit to a mono-exponential decay, and consequently Equation (1) was used to fit the experimental data. In all fits, the integer k was equal to 2 except for the data from the experiment performed at 40 °C after the shear rate of 60 s^{-1} (40 wt% sample) where $k = 3$. For all cases, only the diffusion coefficient with the highest f_n value was considered, as the other diffusion coefficient was attributed to the slight structural heterogeneities across the sample.[28] At 40 °C after 60 s^{-1} (40 wt% sample), two diffusion coefficients were considered and a third excluded (having less weight). The diffusion experiments were performed before and after the applied shear flow in situ. All experiments were recorded after 100 000 strain units, except at the shear rate of 2 s^{-1} for which the experiments were recorded after 40 000 strain units. Figure 9 shows the concentric cylinder flow NMR Couette device and the relative axis frame used in the above discussion. For ideal planar lamellae oriented with the layers parallel to the flow direction, D^z (D along the vorticity direction) and D^y (D along the velocity direction) are expected to be free, whereas along the velocity gradient direction, D^x is expected to be restricted.

The temperature was kept constant using the conventional Bruker temperature control, that is, dry air was used as variable temperature control gas. The sample was allowed to equilibrate at each desired temperature for 20 min before acquisition. Sample temperatures were within ±0.4 °C of the desired temperature, which was verified once prior to the experiments using an external thermocouple loaded into an NMR Couette cell.

Rheology

Rheology measurements were performed using a Physica UDS 200 shear-stress-controlled rheometer (Anton Paar, Ostfildern, Germany) equipped with a Couette cylinder geometry (inner diameter 25 mm, gap 1 mm). The temperature was controlled using a water circulator apparatus (±0.2 °C). To prevent evaporation, measuring geometries were surrounded by a solvent trap containing water. In order to verify the results, a ARES RSF III rheometer (Rheometric Scientific, Piscataway, NJ, USA) equipped with a Couette cylinder geometry (diameter 32 mm, gap 1 mm) was used. Transient experiments were performed by step-rate tests in the range 0.1–100 s^{-1} to construct flow curves at 24, 34 and 40 °C. The shear rate $\dot{\gamma}$ is defined as the ratio between the velocity over the gap, and the shear stress is defined as the macroscopic force divided by the surface.

Under steady shear, non-Newtonian fluids exhibit a variety of nonlinear responses, including yield stress, shear thinning, and shear thickening. For a wide variety of shear-thinning or shear-thickening fluids, a power law can adequately describe the relationship between viscosity and shear rate [Eq. (3)]:

$$\eta \propto \dot{\gamma}^{(n-1)} \tag{3}$$

where η is the apparent viscosity also called transient or shear viscosity. For a Newtonian liquid $n=1$, and for shear-thinning and shear-thickening liquids $n<1$ and $n>1$, respectively.

Flow SANS

SANS experiments were performed on the SANS-II beamline at the Swiss Spallation Neutron Source (SINQ) at the Paul Scherrer Institute (Switzerland).[49,50] The sample was held in a Couette cell with an inner rotating cylinder of 29 mm diameter and a gap of 1 mm. The measurements were performed at a shear rate of 10 and 60 s^{-1} at temperatures greater than 40 °C. The neutron beam traversed the shear cell radially, through the cylinder center (i.e. the scattering was observed in the vorticity–velocity gradient plane). The neutron wavelength was 6.02 Å, and the sample-to-detector distance was 1.2 m, covering a q value range of 0.027–0.24 $Å^{-1}$. The raw data were corrected for empty cell scattering and the intensity was normalized by calibration with incoherent water scattering. In the flow SANS experiments, evaporation was avoided by using a sealed Couette cell.

Acknowledgements

We thank the Paul Scherrer Institute for access to the SANS-II beamline of SINQ. This work was also co-financed by the European Commission, European Social Fund, and the Region of Calabria. The authors are solely responsible for this article, and the European Commission and the Region of Calabria are not responsible for any use that may be made of the information contained herein. We acknowledge financial support from the European Commission under the Seventh Framework Program by means of the grant agreement for the Integrated Infrastructure Initiative no. 262348 European Soft Matter Infrastructure (ESMI).

Keywords: dynamic phase diagram · lamellar phase · phase coexistence · shear-induced transitions · vesicles

[1] W. J. Gibbs, *Trans. Conn. Acad. Arts Sci.*, **1875 – 1878**.
[2] R. Angelico, A. Ceglie, G. Colafemmina, F. Lopez, S. Murgia, U. Olsson, G. Palazzo, *Langmuir* **2005**, *21*, 140 – 148.
[3] K. Holmberg, B. Jönsson, B. Kronberg, B. Lindman, *Surfactants and Polymers in Aqueous Solution*, John Wiley & Sons, New York, **2003**, Ch. 4.
[4] F. Cuomo, F. Lopez, R. Angelico, G. Colafemmina, A. Ceglie, *Colloids Surf. B* **2008**, *64*, 184 – 193.
[5] C. Oliviero, L. Coppola, R. Gianferri, I. Nicotera, U. Olsson, *Colloids Surf. A* **2003**, *228*, 85 – 90.
[6] L. Gentile, M. A. Behrens, S. Balog, K. Mortensen, G. A. Ranieri, U. Olsson, *J. Phys. Chem. B* **2014**, *118*, 3622 – 3629.
[7] L. Gentile, B. F. B. Silva, S. Balog, K. Mortensen, U. Olsson, *J. Colloid Interface Sci.* **2012**, *372*, 32 – 39.
[8] C. R. Safinya, E. B. Sirota, R. F. Bruinsma, C. Jeppesen, R. J. Plano, L. J. Wenzel, *Science* **1993**, *261*, 588 – 591.
[9] T. D. Le, U. Olsson, K. Mortensen, J. Zipfel, W. Richtering, *Langmuir* **2001**, *17*, 999 – 1009.
[10] T. D. Le, U. Olsson, K. Mortensen, *Phys. Chem. Chem. Phys.* **2001**, *3*, 1310 – 1316.
[11] B. Medronho, S. Fujii, W. Richtering, M. G. Miguel, U. Olsson, *Colloid Polym. Sci.* **2005**, *284*, 317 – 321.
[12] M. Bergmeier, M. Gradzielski, H. Hoffmann, K. Mortensen, *J. Phys. Chem. B* **1999**, *103*, 1605 – 1617.
[13] B. Medronho, J. Brown, M. Graça Miguel, C. Schmidt, U. Olsson, P. Galvosas, *Soft Matter* **2011**, *7*, 4938 – 4947.
[14] J. Bergenholtz, N. J. Wagner, *Langmuir* **1996**, *12*, 3122 – 3126.
[15] S. Müller, C. Börsching, W. Gronski, C. Schmidt, D. Roux, *Langmuir* **1999**, *15*, 7558 – 7564.
[16] F. Nettesheim, J. Zipfel, U. Olsson, F. Renth, P. Lindner, W. Richtering, *Langmuir* **2003**, *19*, 3603 – 3618.
[17] Y. Suganuma, M. Imai, T. Kato, U. Olsson, T. Takahashi, *Langmuir* **2010**, *26*, 7988 – 7995.
[18] M. Ito, Y. Kosaka, Y. Kawabata, T. Kato, *Langmuir* **2011**, *27*, 7400 – 7409.
[19] L. Coppola, L. Gentile, I. Nicotera, C. Oliviero Rossi, G. A. Ranieri, *Langmuir* **2010**, *26*, 19060 – 19065.
[20] L. Gentile, C. Oliviero Rossi, U. Olsson, G. A. Ranieri, *Langmuir* **2011**, *27*, 2088 – 2092.
[21] L. Gentile, K. Mortensen, C. Oliviero Rossi, U. Olsson, G. A. Ranieri, *J. Colloid Interface Sci.* **2011**, *362*, 1 – 4.
[22] L. Gentile, C. Oliviero Rossi, U. Olsson, *J. Colloid Interface Sci.* **2012**, *367*, 537 – 539.
[23] O. Diat, D. Roux, *J. Phys. II* **1993**, *3*, 9 – 14.
[24] D. Roux, F. Nallet, O. Diat, *Europhys. Lett.* **1993**, *24*, 53 – 58.
[25] W. Richtering, *Prog. Colloid Polym. Sci.* **1997**, *104*, 90.
[26] J. Zipfel, W. Richtering, P. Lindner, *Prog. Colloid Polym. Sci.* **1998**, *110*, 139 – 143.
[27] J. Zipfel, J. Berghausen, P. Lindner, W. Richtering, *J. Phys. Chem. B* **1999**, *103*, 2841 – 2849.
[28] B. Medronho, U. Olsson, C. Schmidt, P. Galvosas, *Z. Phys. Chem.* **2012**, *226*, 1293 – 1313.
[29] B. Medronho, S. Shafaei, R. Szopko, M. G. Miguel, U. Olsson, C. Schmidt, *Langmuir* **2008**, *24*, 6480 – 6486.
[30] L. Gentile, M. A. Behrens, L. Porcar, P. Butler, N. J. Wagner, U. Olsson, *Langmuir* **2014**, *30*, 8316 – 8325.
[31] S. Fujii, W. Richtering, *Soft Matter* **2013**, *9*, 5391 – 5400.
[32] J. Zipfel, J. Berghausen, G. Schmidt, P. Lindner, P. Alexandridis, M. Tsianou, W. Richtering, *Phys. Chem. Chem. Phys.* **1999**, *1*, 3905 – 3910.
[33] A. K. Gurnon, P. D. Godfrin, N. J. Wagner, A. P. R. Eberle, P. Butler, L. Porcar, *J. Visualized Exp.* **2014**, *84*, e51068.
[34] M. W. Liberatore, F. Nettesheim, N. J. Wagner, *Phys. Rev. E* **2006**, *73*, 020504(R).
[35] H. F. Mahjoub, C. Bourgaux, P. Sergot, M. Kleman, *Phys. Rev. Lett.* **1998**, *81*, 2076 – 2079.
[36] L. Porcar, W. A. Hamilton, P. D. Butler, G. G. Warr, *Phys. B* **2004**, *350*, e963 – e966.
[37] A. Léon, D. Bonn, J. Meunier, A. Al-Kahwaji, H. Kellay, *Phys. Rev. Lett.* **2001**, *86*, 938 – 941.
[38] M. Pinna, A. V. Zvelindovsky, *Soft Matter* **2008**, *4*, 316 – 327.
[39] R. Eskimergen, K. Mortensen, M. Vigild, *Macromolecules* **2005**, *38*, 1286 – 1291.
[40] P. D. Olmsted, C.-Y. D. Lu, *Faraday Discuss.* **1999**, *112*, 183 – 194.
[41] R. G. Laughlin in *Micelles, Microemulsions, and Monolayers* (Ed.: D. O. Shah), Marcel Dekker, New York, **1998B**, Ch. 3, 81 – 82.
[42] S. Fujii, W. Richtering, *Eur. Phys. J. E* **2006**, *19*, 139 – 148.
[43] J. Mitchell, G. J. T. Tiddy, L. Waring, T. Bostock, M. P. McDonald, *J. Chem. Faraday Trans.* **1983**, *79*, 975 – 1000.
[44] G. Briganti, A. L. Segre, D. Capitani, C. Casieri, C. La Mesa, *J. Phys. Chem. B* **1999**, *103*, 825 – 830.
[45] H. Edlund, A. Khan, C. La Mesa, *Langmuir* **1998**, *14*, 3691 – 3697.
[46] D. Bernin, V. Koch, M. Nyde, D. Topgaard, *PLoS One* **2014**, *9*, e98752.
[47] S. J. Gibbs, C. S. Johnson, Jr., *J. Magn. Reson.* **1991**, *93*, 395 – 402.
[48] E. O. Stejskal, J. E. Tanner, *J. Chem. Phys.* **1965**, *42*, 288 – 292.
[49] P. Strunz, K. Mortensen, S. Janssen, *Phys. B* **2004**, *350*, E783.
[50] K. Mortensen, K. Almdal, F. S. Bates, K. Koppi, M. Tirell, B. Nordén, *Phys. B* **1995**, *213*, 682 – 684.

Received: March 18, 2015